Coherence temperature in the diluted periodic Anderson model

N. C. Costa,[1] T. Mendes-Santos,[2] T. Paiva,[1] N. J. Curro,[3] R. R. dos Santos,[1] and R. T. Scalettar[3]
[1]*Instituto de Física, Universidade Federal do Rio de Janeiro, Caixa Postale 68.528, 21941-972 Rio de Janeiro RJ, Brazil*
[2]*The Abdus Salam International Centre for Theoretical Physics, strada Costiera 11, 34151 Trieste, Italy*
[3]*Department of Physics, University of California, Davis, California 95616, USA*

(Received 21 December 2018; revised manuscript received 17 April 2019; published 9 May 2019)

The Kondo and periodic Anderson model (PAM) are known to provide a microscopic picture of many of the fundamental properties of heavy-fermion materials and, more generally, a variety of strong correlation phenomena in $4f$ and $5f$ systems. In this paper, we apply the determinant quantum Monte Carlo method to include disorder in the PAM, specifically the removal of a fraction x of the localized orbitals. We determine the evolution of the coherence temperature T^*, where the local moments and conduction electrons become entwined in a heavy-fermion fluid, with x and with the hybridization V between localized and conduction orbitals. We recover several of the principal observed trends in T^* of doped heavy fermions, and we also show that, within this theoretical framework, the calculated nuclear magnetic resonance relaxation rate tracks the experimentally measured behavior in pure and doped $CeCoIn_5$. Our results contribute to important issues in the interpretation of local probes of disordered, strongly correlated systems.

DOI: 10.1103/PhysRevB.99.195116

I. INTRODUCTION

Materials poised at the cusp of magnetic to nonmagnetic phase boundaries exhibit a myriad of complex properties. As systems ranging from cuprate superconductors [1,2] to heavy fermions [3–5] and iron pnictides [6,7] are moved with pressure, chemical doping, or temperature away from a regime where magnetic order is dominant, an incredible variety of alternate patterns of spin, charge, and pairing emerges. A description of the resulting competition has been an ongoing challenge to the condensed-matter community [8].

To address these phenomena, nuclear magnetic resonance (NMR) has been extensively used to explore local microscopic properties of correlated materials, providing great insight into their nature [9–11]. In particular, NMR experiments have determined the energy scale at which a heavy-fermion state emerges, i.e., when $4f$ electrons become delocalized. This scale has been associated [12–18] with a *coherence temperature,* T^*, whose signature appears, e.g., as an anomaly in Knight shift (KS) measurements: while for normal metals the KS tracks the magnetic susceptibility, for most heavy-fermion materials this tracking breaks down below a certain temperature, which is identified with T^* [12,13]. The presence of several distinct contributions to the magnetic susceptibility in these materials, in particular the one from a singlet d-f channel that delocalizes $4f$-electrons, leads to this anomaly, signaling the emergence of a heavy-fermion state. Remarkably, when the KS anomaly is singled out by removing the high-temperature contribution to the susceptibility, many heavy-fermion materials exhibit a universal behavior for temperatures below T^* [12,13]. The coherence temperature is evident in multiple experimental probes, including transport, thermodynamic, and tunneling measurements, but its microscopic origin, and its relation to the Kondo screening temperature, remain open questions [17–19].

Additional complexity is introduced by added chemical impurities [19–23], so that treating the effects of disorder is essential to understand many of the properties of correlated electron materials. Randomness is central to the emergent physics since it acts to limit the growth of charge-ordered regions [24]. Likewise, dopant disorder can stabilize localized antiferromagnetic (AF) regions, explaining the persistence of AF even deep in the d-wave phase [25]. A similar phenomenon occurs in heavy-fermion materials where AF long-range order is induced via Cd doping of $CeCoIn_5$ [22,26]. Of particular interest is the crossover between Kondo screening in the single-impurity limit and collective screening with intersite interactions among multiple sites in a lattice.

A powerful approach to investigate these crossover regimes is to systematically replace the f-sites with nonmagnetic atoms. This leads to inhomogeneities in the magnetic response, with some spatial regions favoring strong spin correlations, while in others a paramagnetic behavior is preferred. Thus, instead of having a single external parameter that globally tunes a system through a magnetic/nonmagnetic boundary, one should also investigate how the physical quantities behave in the presence of internal and highly inhomogeneous degrees of freedom. One expects NMR quantities like T^* and the spin-lattice relaxation rate to have a strong dependence with impurity doping (e.g., La substitution on Ce-based compounds) and even acquire a distribution of values depending on the local environment of the nuclei [27–33]. Indeed, NMR and scanning tunneling microscopy (STM) measurements on the cuprates have examined the links between charge order, superconductivity, and pseudogap physics in the cuprates.

From a theoretical point of view, the nature of these emergent phenomena may be described by simplified models that take into account their most fundamental mechanisms, such as the periodic Anderson model (PAM) [34–38] and the closely related Kondo lattice model [39–43], which consider

weakly correlated "conduction" electrons hybridized with strongly correlated "localized" ones. Tuning the strength of the hybridization in these models leads to a quantum phase transition (QPT), in which the ground state evolves from an antiferromagnetic (AF) ordering to a spin liquid state. Recent numerical work on the homogeneous PAM has captured the KS anomaly and provided T^* by quantitatively characterizing the different orbital contributions to the global susceptibility [44,45]. In the context of impurity doping [46], the PAM successfully describes the enhancement of AF correlations around doped impurities in $CeCo(In_{1-x}Cd_x)_5$ [47–49], and it also provides evidence of a magnetic suppression when nonlocal hybridization terms are included [50,51], as in the case of $CeCo(In_{1-x}Sn_x)_5$ [23,52].

Here we study the combination of randomness and strong interactions with an exact numerical approach, which allows for "real-space imaging" of spin correlations. We investigate the behavior of the coherence temperature and NMR quantities in *chemically doped* heavy-fermion materials, such as in $Ce_{1-x}La_xCoIn_5$, with quantum simulations that accurately incorporate sites with missing magnetic moments. Our focus is on whether the calculated trends of these quantities resemble those from experimental NMR measurements [31] on the evolution with impurity doping and external parameters. To this end, we extend previous [44] determinant quantum Monte Carlo (DQMC) simulations to treat the *randomly diluted* PAM (dPAM), as presented in the next section. In Secs. III and IV we discuss our findings, from which our key results are as follows: (i) the KS anomaly exhibits a universal scaling behavior below T^*, even in the presence of disorder; (ii) T^* increases with hybridization V (or pressure); and (iii) it linearly decreases with impurity concentration x. Finally, (iv) the NMR relaxation rate, $1/T_1$, exhibits a strongly inhomogeneous pattern throughout the lattice. These demonstrate that several of the most fundamental conclusions of NMR experiments can be predicted, including the scaling behavior of T^*. In Sec. V we summarize our main conclusions.

II. MODEL AND METHOD

The Hamiltonian for the dPAM reads [53]

$$\mathcal{H} = -t\sum_{\langle \mathbf{i},\mathbf{j}\rangle,\sigma}(c^\dagger_{\mathbf{i}\sigma}c_{\mathbf{j}\sigma}+\text{H.c.}) - \sum_{\mathbf{i},\sigma}V_{\mathbf{i}}\,(c^\dagger_{\mathbf{i}\sigma}f_{\mathbf{i}\sigma}+\text{H.c.}) - \mu\sum_{\mathbf{i},\sigma,\alpha}n^\alpha_{\mathbf{i}\sigma} + \sum_{\mathbf{i}}U^f_{\mathbf{i}}\left(n^f_{\mathbf{i}\uparrow}-\frac{1}{2}\right)\left(n^f_{\mathbf{i}\downarrow}-\frac{1}{2}\right), \quad (1)$$

where the sums run over a two-dimensional square lattice, with $\langle \mathbf{i},\mathbf{j}\rangle$ denoting nearest-neighbor sites, and $\alpha = c$ or f; the notation for the operators is standard. The first term corresponds to the hopping of conduction electrons (the hopping integral, t, sets the energy scale), while the last term describes the Coulomb repulsion on localized f-orbitals. The hybridization between these two orbitals is modeled by a site-dependent hopping $V_{\mathbf{i}}$

Here we consider *full orbital dilution*, in which we randomly set $U_{\mathbf{i}} = V_{\mathbf{i}} = 0$ on a fraction x of the sites. Physically, this is equivalent to completely removing f-orbitals, similarly to the replacement of a magnetic $4f^1$ Ce atom by a $4f^0$ La one in $CeCoIn_5$, which locally suppresses both the moment on the f-orbital and the possibility of c-f mixing (due to the distance of the La level from the Fermi energy).

The DQMC method [54–59] employed here to solve Eq. (1) is an unbiased technique commonly used to investigate Hubbard-like Hamiltonians: it maps a d-dimensional quantum system in a classical $(d+1)$-dimensional one, via the inclusion of an imaginary-time coordinate. Within this approach, one separates the one-body ($\hat{\mathcal{K}}$) and two-body ($\hat{\mathcal{P}}$) pieces in the partition function by using the Trotter-Suzuki decomposition, i.e., by defining $\beta = L_\tau \Delta\tau$, with L_τ being the number of imaginary-time slices, and $\Delta\tau$ is the discretization grid. Then

$$\mathcal{Z} = \text{Tr}\, e^{-\beta\hat{\mathcal{H}}} = \text{Tr}\,[(e^{-\Delta\tau(\hat{\mathcal{K}}+\hat{\mathcal{P}})})^{L_\tau}] \approx \text{Tr}\,[e^{-\Delta\tau\hat{\mathcal{K}}}e^{-\Delta\tau\hat{\mathcal{P}}}e^{-\Delta\tau\hat{\mathcal{K}}}e^{-\Delta\tau\hat{\mathcal{P}}}\cdots], \quad (2)$$

with an error proportional to $(\Delta\tau)^2$. This is exact in the limit $\Delta\tau \to 0$. The resulting partition function is rewritten in quadratic (single-body) form through a discrete Hubbard-Stratonovich transformation (HST) on the two-body terms, $e^{-\Delta\tau\hat{\mathcal{P}}}$. This HST introduces discrete auxiliary fields with components on each of the space and imaginary-time lattice coordinates, which are sampled by Monte Carlo techniques. In this work, we choose $t\Delta\tau = 0.1$, so that the error from the Trotter-Suzuki decomposition is less than, or comparable to, that from the Monte Carlo sampling. DQMC is able to measure a general set of single- and two-particle response functions, such as susceptibilities, which can be directly compared with experimental results.

Although numerically exact, DQMC is constrained by the infamous minus-sign problem [57,59], which restricts our analyses to the half-filling case, i.e., when both c- and f-orbitals have $\langle n^{c,f}_{\mathbf{i},\sigma}\rangle = 1/2$. Determinant quantum Monte Carlo is especially well-matched to analyze the problem of disorder and the local structures that form around an impurity, since it is formulated in real space. Furthermore, many types of randomness, such as local variations in hybridization, on-site repulsion, and site removal, do not affect particle-hole symmetry. Therefore, there is no sign problem at half-filling, regardless of the presence of disorder (dilution) on the lattice. This allows us to investigate the behavior of correlations in all temperature scales.

To connect with NMR measurements, the central quantities of interest are magnetic susceptibilities, from which the Knight shift and spin-lattice relaxation rate are obtained; see below. Due to the presence of two orbitals, the total spin on a given site $\mathbf{i}$ is $\mathbf{S}_{\mathbf{i}} = \mathbf{S}^c_{\mathbf{i}} + \epsilon_{\mathbf{i}}\mathbf{S}^f_{\mathbf{i}}$, with $\epsilon_{\mathbf{i}} \equiv 1$ at sites containing f-orbitals, and 0 otherwise. Thus, the total magnetic susceptibility is given by

$$\chi = \chi_{cc} + 2\chi_{cf} + \chi_{ff}, \quad (3)$$

where

$$\chi_{\alpha\alpha'} = \frac{1}{N_s}\sum_{\mathbf{ij}} Q^{\alpha\alpha'}_{\mathbf{ij}} \int_0^\beta d\tau\, \langle \mathbf{S}^\alpha_{\mathbf{i}}(\tau)\cdot\mathbf{S}^{\alpha'}_{\mathbf{j}}(0)\rangle. \quad (4)$$

Here $\mathbf{S}^\alpha_{\mathbf{i}}(\tau) = e^{\tau\mathcal{H}}\mathbf{S}^\alpha_{\mathbf{i}}(0)\,e^{-\tau\mathcal{H}}$, with $\alpha, \alpha' = c$ or f, and $Q^{\alpha\alpha'}_{\mathbf{ij}} = [(\delta_{\alpha,c} + \epsilon_{\mathbf{i}}\epsilon_{\mathbf{j}}\delta_{\alpha,f})\delta_{\alpha,\alpha'} + (\epsilon_{\mathbf{i}}\delta_{\alpha,f}\delta_{\alpha',c} + \epsilon_{\mathbf{j}}\delta_{\alpha,c}\delta_{\alpha',f})]$; the number of lattice sites is $N_s = L \times L$. Similarly, the Knight

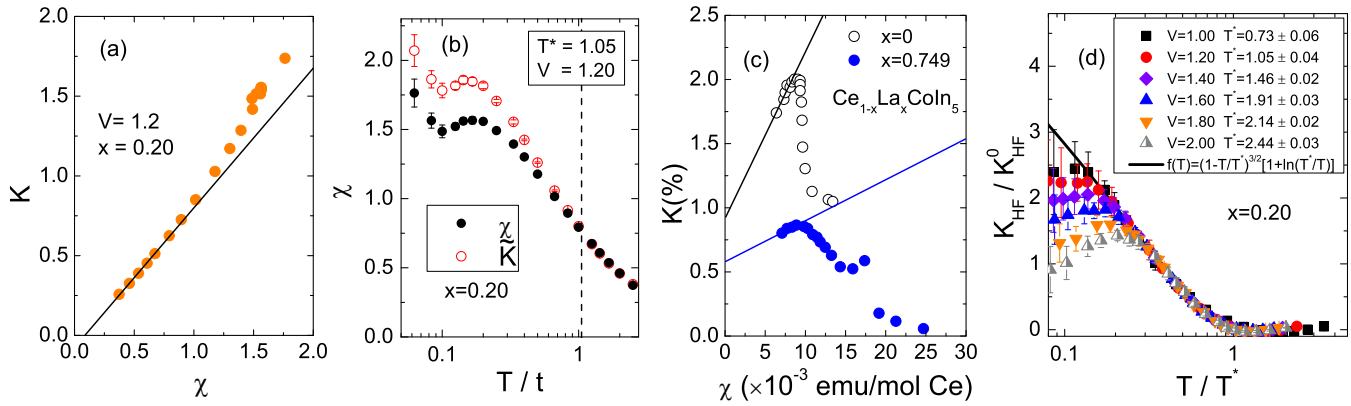

FIG. 1. (a) Knight shift as a function of total susceptibility χ. (b) χ and the renormalized Knight shift $\tilde{K}$ as a function of temperature, for $V/t = 1.2$ and $x = 0.20$. The vertical dashed line defines $T^*/t = 1.05$ (see text). (c) Experimental NMR results for $Ce_{1-x}La_xCoIn_5$ reproduced from Ref. [31]. (d) Data collapse of DQMC results for the KS anomaly, $K_{\rm HF}$, for $T \lesssim T^*$. Here, and in all subsequent figures, when not shown, error bars are smaller than the symbol size.

shift is

$$K = A\chi_{cc} + (A+B)\chi_{cf} + B\chi_{ff} + K_0, \tag{5}$$

where A (B) corresponds to the hyperfine coupling between the nuclear spin of In(1) atoms and conduction (localized) electrons. K_0 is a temperature-independent term arising from orbital and diamagnetic contributions to K, which we set to zero. Recall that the Knight shift is a local quantity, which depends on the distribution of nearest-neighbor site (Ce or La) moments to the central In(1) atom [31]. Thus, our data correspond to the average K of representative sites that couple to both $\mathbf{S}^c$ and $\mathbf{S}^f$ spins. Since the hyperfine couplings are generally different [12,60], and strongly material-dependent, we follow a previous study [44] and take $A/B = 0.3$; general trends are not sensitive to the precise choice of A/B [44]. Our simulations capture qualitative features of χ, K, and $1/T_1$, but not material-specific details. In what follows, our DQMC data are averages over 20–30 different disorder configurations on a 10×10 square lattice, and $U^f/t = 4$. Most of our results were obtained for $V \geqslant 1$, corresponding to the singlet region for the clean PAM [37,38].

III. THE COHERENCE TEMPERATURE

At high temperatures, localized electrons are weakly coupled to conduction bands, so the contribution of χ_{cc} and χ_{cf} may be disregarded. As a result, the Knight shift [Eq. (5)] tracks the *localized* electron susceptibility and, under the same assumptions, the total susceptibility χ as well. Following the procedure adopted in analyses of the experiments, we perform a linear fit to our DQMC Knight shift data as a function of the susceptibility in the high-temperature region, i.e., $K = B_{\rm eff}\chi + K_{0,\rm eff}$ [see Fig. 1(a)]. Next, we define the renormalized KS,

$$\tilde{K} \equiv (K - K_{0,\rm eff})/B_{\rm eff}, \tag{6}$$

which is equal to χ at high temperatures. This equality holds as long as the c-f singlet channel is small. However, since $(A+B)/B \neq 2$, $\tilde{K}$ fails to track χ when χ_{cf} becomes relevant: the associated energy scale is T^*; see Fig. 1(b). In this way the Knight shift, which detects the contribution of a c-f channel (hence the presence of delocalized $4f$ electrons), provides an important tool to investigate the emergence of a heavy-fermion state and its temperature scale. The KS anomaly persists even in strongly diluted materials, as displayed in Fig. 1(c), for the heavy-fermion $Ce_{1-x}La_xCoIn_5$, with $x \approx 0.75$.

It is worth emphasizing that the continued appearance of the coherence temperature in the presence of disorder at a value similar to that of the pure system [44,61] is a nontrivial observation. Indeed, electrons in unpaired orbitals (which survive dilution) are known to give large contributions to the susceptibility, regardless of whether they are conducting or localized [49,62,63]. This could, in principle, significantly affect the assumptions under which $\tilde{K}$ would track χ, hence the value of T^* as well. As we shall see, these effects are more relevant at very low temperatures, due to the possibility of long-range order setting in the ground state. The relatively weak dependence of the NMR quantities with dilution, as presented in Figs. 1(a)–1(c), is an important step toward a *global* understanding of T^* in diluted systems.

Within a two-fluid model [12,13,28,64,65], one singles out the "heavy-fermion fluid" contribution to the KS by subtracting its "normal" (high-temperature) contribution, i.e.,

$$K_{\rm HF} \equiv B_{\rm eff}(\tilde{K} - \chi). \tag{7}$$

Remarkably, experimental results suggest a universal behavior of $K_{\rm HF}$ for many different heavy-fermion materials,

$$\frac{K_{\rm HF}(T)}{K^0_{\rm HF}} = f(T) \equiv (1 - T/T^*)^{3/2}[1 + \ln(T^*/T)], \tag{8}$$

where $K^0_{\rm HF}$ and T^* depend on the specific material, and on external parameters. We use this phenomenological scaling form for a more accurate estimate of T^* through the collapse of our DQMC data, as shown in Fig. 1(d).

The behavior of the KS in Fig. 1, in particular its scaling behavior [Fig. 1(d)], provides robust evidence that DQMC simulations qualitatively reproduce trends observed experimentally, even in the presence of disorder. We now turn our attention to the dependence of T^* with external parameters, such as the hybridization, V, which is tuned in experiments

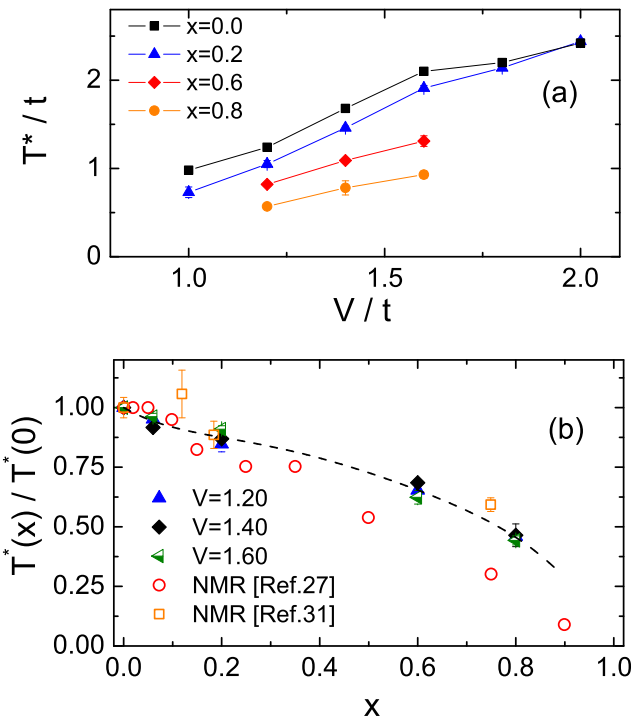

FIG. 2. (a) The coherence temperature T_* as a function of V for different dilution fractions x. (b) Dependence of T^* on f-orbital dilution x in the PAM. Data for different c-f hybridizations V are normalized to their clean ($x = 0$) system value. Experimental NMR results on $Ce_{1-x}La_xCoIn_5$ are reproduced from Ref. [27] (open red circles) and Ref. [31] (open orange squares). The black dashed line is a guide to the eye for DQMC data. The DQMC results are in excellent qualitative (and, indeed, almost quantitative) agreement with experiment.

by applying pressure. Figure 2(a) displays the behavior of T^* as a function of V for different impurity concentrations, x. Regardless of the level of disorder, the coherence temperature increases monotonically with V. This reproduces fundamental features of NMR measurements (e.g., for $CeRhIn_5$ [66]): larger hybridization increases the probability of a hopping from f-orbitals to conduction ones, which in turn increases the energy scale ($\sim V^2/U^f$).

The effect of dilution on T^* is already apparent in Fig. 2(a): although the clean and disordered cases share the same qualitative trend, the value of T^* decreases with x. This reduction in the coherence temperature with f-orbital dilution reflects a crossover between dense and diluted Kondo regimes; that is, the material goes from a heavy-fermion state at small x to a single-impurity Kondo regime at $x \approx 1 - \epsilon$, with $\epsilon \ll 1$. To further emphasize this crossover, Fig. 2(b) displays T^* as a function of dilution for different values of hybridization. Notice that T^* has a (roughly) linear dependence with x, with $T^* \neq 0$ even at strong dilution. Our DQMC predictions are in good agreement with recent NMR results for $Ce_{1-x}La_xCoIn_5$, as shown in Fig. 2(b); see Ref. [31]. Data from early attempts to measure T^* in $Ce_{1-x}La_xCoIn_5$ (see, e.g., Ref. [27]) are also included in Fig. 2(b): they also display a monotonic decrease of the coherence temperature with La doping.

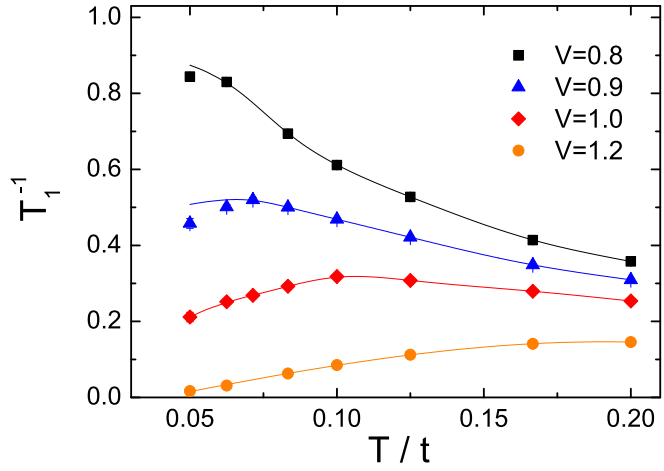

FIG. 3. Spin-lattice relaxation rate of the clean PAM as a function of temperature, for different hybridizations V. Solid lines are guides to the eye.

IV. RELAXATION TIME

The NMR relaxation rate is defined as (see, e.g., Ref. [10])

$$T_1^{-1} = \gamma^2 k_B T \lim_{\omega\to 0} \sum_{\mathbf{q}} A^2(\mathbf{q}) \frac{\chi''(\mathbf{q},\gamma)}{\hbar\omega}, \tag{9}$$

where $A^2(\mathbf{q})$ is the square of the Fourier transform of the hyperfine interaction, and γ is the gyromagnetic ratio. The latter is related to the nuclear magnetic moment by $\gamma\hbar = g\mu_N\sqrt{I(I+1)}$, with μ_N being the nuclear magneton, g the nuclear g-factor, and I the nuclear spin. T_1^{-1} quantifies a characteristic time in which a component of the nuclear spin (of a given site) reaches equilibrium after an external perturbation (magnetic-field pulse). It is a dynamical (real frequency) quantity whose numerical evaluation usually requires an analytic continuation of the imaginary-time DQMC data. Instead, we use an approximation to this procedure [67],

$$\frac{1}{T_1} = \frac{1}{\pi^2 T} \sum_{\mathbf{i}} \langle S_{\mathbf{i}}(\tau = \beta/2) S_{\mathbf{i}}(0)\rangle \,. \tag{10}$$

As a benchmark for our results for the diluted case, we first examine the behavior of T_1^{-1} for the clean ($x = 0$) system. Previous DQMC studies [36,37] of the PAM have provided evidence of a QPT from an antiferromagnetically (AFM) ordered ground state to a spin liquid phase at $V_c \approx 1.0$. Then, one expects that the behavior of T_1^{-1} for decreasing temperatures should reflect the properties of these different ground states [63]. Figure 3 displays the behavior of the relaxation rate as a function of temperature for different values of V. Here we show the results from extrapolating data for lattice sizes $L = 8$, 10, and 12 to $L \to \infty$. Within the AFM phase, $V/t = 0.8$ or 0.9, T_1^{-1} approaches a finite nonzero value as $T \to 0$, consistent with the absence of a spin gap, i.e., the presence of spin-wave excitations. On the other hand, for larger V, T_1^{-1} decreases monotonically when T is lowered, reflecting a spin-gapped (spin liquid) ground state. Notice that the change in behavior of T_1^{-1} occurs around $V/t \sim 1.0$, in line with the V_c reported in Ref. [37].

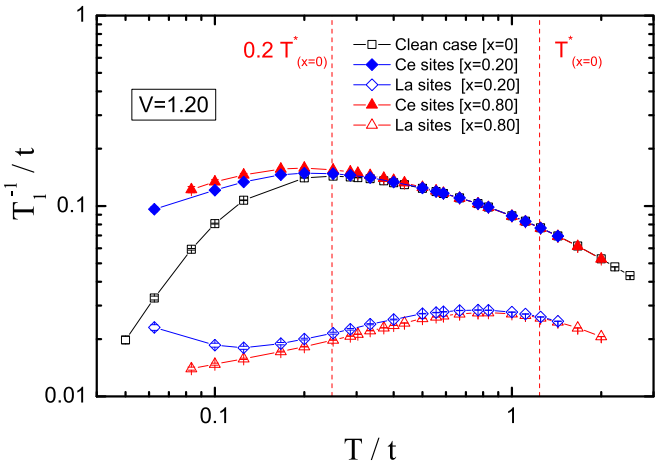

FIG. 4. Local contributions to the spin-lattice relaxation rate for $x = 0.20$ and 0.80, as compared with the clean case ($x = 0$). Vertical red dashed lines correspond to T^* and $0.2T^*$ for $x = 0$, and $V/t = 1.20$.

Turning to the disordered case, the lack of translational symmetry requires the analysis of *local* contributions to T_1^{-1} by considering two species of sites: (i) Ce sites, those with an active f-orbital, and (ii) La sites, those which had their f-orbitals removed. Accordingly, we define T_1^{-1} for Ce and La as the average over their individual contributions, i.e., we average over the available sites of each type, and subsequently we average over disorder configurations. Figure 4 displays the behavior of the local T_1^{-1} for fixed $V/t = 1.2$ and for different concentrations. For reasons that will become apparent below, we separate the discussion of Fig. 4 into two regimes: intermediate temperatures, $T \sim T^*$, and low temperatures, $T \ll T^*$, when properties reflect the dominant correlations in the ground state. In the intermediate-temperature range, we note that data for the spin relaxation rate on Ce sites for the clean case and for both dilution cases ($x = 0.20$ and 0.80) are almost indistinguishable; for the La sites, data for these same concentrations are also nearly identical, though much smaller than those for the Ce sites. When compared with the experimental results in Fig. 10 of Ref. [31], we see that the same data grouping occurs, and that the decrease of T_1^{-1} as the temperature decreases (below the broad maxima) is also present; the difference in magnitude between data for Ce and La sites is also noticeable. These features, therefore, provide evidence that the T_1^{-1} distribution is quite inhomogeneous throughout the lattice, with Ce sites behaving as in the clean case even for strong dilution. A possible explanation for this inhomogeneity may be a local nature of singlet formation, i.e., singlets have a short correlation length.

In the low-temperature regime, the strong attenuation observed in our DQMC results for the pure case is due to the spin-gapped ground state. For the diluted systems, however, our T_1^{-1} data on Ce sites seem to converge to finite values as T decreases, consistent with gapless behavior due to either enhanced magnetic correlations or metallic (Pauli-like) behavior, depending on the degree of dilution. It is worth noting that the T_1^{-1} for $x = 0.20$ and 0.80 have similar behavior, despite the large difference in the disorder strength. In fact, previous theoretical works [68,69] have suggested that the dense Kondo regime occurs just for $n_c \approx n_f$, while the diluted Kondo regime is established for a wide region of $n_c < n_f$, which is in line with our findings here. The difference between these two dilutions occurs only for La sites at very low temperatures. The data for La sites when $x = 0.20$ show that T_1^{-1} increases with decreasing temperatures for $T/t \lesssim 0.1$, corresponding to an enhancement of magnetic correlations on these sites, a behavior also found for the regularly depleted PAM [49]. We note that the half-filling of our model for dilution may impose a bias toward an AFM ground state, since conduction sites with removed partners are unable to form singlets [63].

V. CONCLUSIONS

In summary, we have presented results for the magnetic susceptibility, Knight shift, and NMR relaxation rate computed using DQMC simulations for the diluted periodic Anderson model. We showed that even in the presence of disorder, the Knight shift anomaly displays a behavior with a phenomenological universal function shared with the clean case. We have also obtained the coherence temperature, T^*, and its dependence on c-f hybridization, V, and with the dilution fraction x. We have found that T^* is a linearly decreasing function of x, reproducing a crucial feature of the experimental results for La-doped $CeCoIn_5$. Finally, we have also discussed the spin-lattice relaxation rate, which is distributed inhomogeneously throughout the lattice. The qualitative agreement of our results with experimental NMR measurements for $Ce_{1-x}La_xCoIn_5$ suggests DQMC is a powerful theoretical tool to model accurately the nature of spin correlations in disordered heavy-fermion materials.

Although we have emphasized the use of DQMC within the context of condensed-matter materials, our work also has important implications for "quantum gas microscopes" and their use to explore ultracold trapped atoms [70–72]. Like the NMR measurements described here, quantum gas microscopy allows the resolution of single atoms, doubly occupied sites, and (local) magnetic order. A central focus is on nonequilibrium properties directly connected to the relaxation times studied here.

ACKNOWLEDGMENTS

N.C.C., T.P., and R.R.dS. were supported by the Brazilian Agencies CAPES, CNPq, and FAPERJ. N.J.C. was supported by NSF, Grants No. DMR-1005393 and No. DMR-1807889, and RTS by Department of Energy, Grant No. DE-SC0014671.

[1] D. J. Scalapino, The case for $d_{x^2-y^2}$ pairing in the cuprate superconductors, Phys. Rep. **250**, 329 (1995).

[2] B. Keimer, S. A. Kivelson, M. R. Norman, S. Uchida, and J. Zaanen, From quantum matter to high-temperature

superconductivity in copper oxides, Nature (London) **518**, 179 (2015).

[3] H. Tou, Y. Kitaoka, K. Asayama, C. Geibel, C. Schank, and F. Steglich, d-wave superconductivity in antiferromagnetic heavy-fermion compound UPd_2Al_3—Evidence from ^{27}Al NMR/NQR studies, J. Phys. Soc. Jpn. **64**, 725 (1995).

[4] P. Coleman, Heavy fermions: Electrons at the edge of magnetism, *Handbook of Magnetism and Advanced Magnetic Materials* (Wiley, New York, 2007).

[5] P. Gegenwart, Q. Si, and F. Steglich, Quantum criticality in heavy-fermion metals, Nat. Phys. **4**, 186 (2008).

[6] A. V. Chubukov, D. V. Efremov, and I. Eremin, Magnetism, superconductivity, and pairing symmetry in iron-based superconductors, Phys. Rev. B **78**, 134512 (2008).

[7] Q. Si, R. Yu, and E. Abrahams, High-temperature superconductivity in iron pnictides and chalcogenides, Nat. Rev. Mater. **1**, 16017 (2016).

[8] E. Dagotto, Complexity in strongly correlated electronic systems, Science **309**, 257 (2005).

[9] Y. Kitaoka, H. Tou, G.-Q. Zheng, K. Ishida, K. Asayama, T. C. Kobayashi, A. Kohda, N. Takeshita, K. Amaya, Y. Onuki, G. Geibel, C. Schank, and F. Steglich, NMR study of strongly correlated electron systems, Physica B **206-207**, 55 (1995).

[10] N. J. Curro, Nuclear magnetic resonance in the heavy fermion superconductors, Rep. Prog. Phys. **72**, 026502 (2009).

[11] R. E. Walstedt, *The NMR Probe of High-Tc Materials and Correlated Electron Systems* (Springer-Verlag, Berlin, 2018).

[12] N. J. Curro, B.-L. Young, J. Schmalian, and D. Pines, Scaling in the emergent behavior of heavy-electron materials, Phys. Rev. B **70**, 235117 (2004).

[13] Y.-F. Yang and D. Pines, Universal Behavior in Heavy-Electron Materials, Phys. Rev. Lett. **100**, 096404 (2008).

[14] Y.-F. Yang and D. Pines, Emergent states in heavy-electron materials, Proc. Natl. Acad. Sci. (USA) **109**, E3060 (2012).

[15] Y.-F. Yang and D. Pines, Quantum critical behavior in heavy electron materials, Proc. Natl. Acad. Sci. (USA) **111**, 8398 (2014).

[16] Y.-F. Yang, D. Pines, and N. J. Curro, Quantum critical scaling and superconductivity in heavy electron materials, Phys. Rev. B **92**, 195131 (2015).

[17] Y.-F. Yang, Z. Fisk, H.-O. Lee, J. D. Thompson, and D. Pines, Scaling the Kondo lattice, Nature (London) **454**, 611 (2008).

[18] Y.-F. Yang, D. Pines, and G. Lonzarich, Quantum critical scaling and fluctuations in Kondo lattice materials, Proc. Natl. Acad. Sci. (USA) **114**, 6250 (2017).

[19] S. Wirth and F. Steglich, Exploring heavy fermions from macroscopic to microscopic length scales, Nat. Rev. Mater. **1**, 16051 (2016).

[20] E. Miranda and V. Dobrosavljević, Disorder-driven non-Fermi liquid behavior of correlated electrons, Rep. Prog. Phys. **68**, 2337 (2005).

[21] S. Kawasaki, M. Yashima, Y. Mugino, H. Mukuda, Y. Kitaoka, H. Shishido, and Y. Ōnuki, Enhancing the Superconducting Transition Temperature of $CeRh_{1-x}Ir_xIn_5$ Due to the Strong-Coupling Effects of Antiferromagnetic Spin Fluctuations: An ^{115}In Nuclear Quadrupole Resonance Study, Phys. Rev. Lett. **96**, 147001 (2006).

[22] S. Seo, X. Lu, J.-X. Zhu, R. R. Urbano, N. Curro, E. D. Bauer, V. A. Sidorov, L. D. Pham, T. Park, Z. Fisk, and J. D. Thompson, Disorder in quantum critical superconductors, Nat. Phys. **10**, 120 (2014).

[23] K. Chen, F. Strigari, M. Sundermann, Z. Hu, Z. Fisk, E. D. Bauer, P. F. S. Rosa, J. L. Sarrao, J. D. Thompson, J. Herrero-Martin, E. Pellegrin, D. Betto, K. Kummer, A. Tanaka, S. Wirth, and A. Severing, Evolution of ground-state wave function in $CeCoIn_5$ upon Cd or Sn doping, Phys. Rev. B **97**, 045134 (2018).

[24] L. Nie, G. Tarjus, and S. Allan Kivelson, Quenched disorder and vestigial nematicity in the pseudogap regime of the cuprates, Proc. Natl. Acad. Sci. (USA) **111**, 7980 (2014).

[25] B. M. Andersen, P. J. Hirschfeld, A. P. Kampf, and M. Schmid, Disorder-Induced Static Antiferromagnetism in Cuprate Superconductors, Phys. Rev. Lett. **99**, 147002 (2007).

[26] L. D. Pham, T. Park, S. Maquilon, J. D. Thompson, and Z. Fisk, Reversible Tuning of the Heavy-Fermion Ground State in $CeCoIn_5$, Phys. Rev. Lett. **97**, 056404 (2006).

[27] S. Nakatsuji, S. Yeo, L. Balicas, Z. Fisk, P. Schlottmann, P. G. Pagliuso, N. O. Moreno, J. L. Sarrao, and J. D. Thompson, Intersite Coupling Effects in a Kondo Lattice, Phys. Rev. Lett. **89**, 106402 (2002).

[28] S. Nakatsuji, D. Pines, and Z. Fisk, Two Fluid Description of the Kondo Lattice, Phys. Rev. Lett. **92**, 016401 (2004).

[29] K. Ohishi, R. H. Heffner, T. U. Ito, W. Higemoto, G. D. Morris, N. Hur, E. D. Bauer, J. L. Sarrao, J. D. Thompson, D. E. MacLaughlin, and L. Shu, Development of the heavy-fermion state in Ce_2IrIn_8 and the effects of Ce dilution in $(Ce_{1-x}La_x)_2IrIn_8$, Phys. Rev. B **80**, 125104 (2009).

[30] F. C. Ragel, P. de V du Plessis, and A. M. Strydom, Dilution and non-Fermi-liquid effects in the CePtIn Kondo lattice, J. Phys.: Condens. Matter **21**, 046008 (2009).

[31] M. Lawson, B. T. Bush, A. C. Shockley, C. Capan, Z. Fisk, and N. J. Curro, Site-specific Knight shift measurements of the dilute Kondo lattice system $Ce_{1-x}La_xCoIn_5$, Phys. Rev. B **99**, 165106 (2019).

[32] D. E. MacLaughlin, O. O. Bernal, R. H. Heffner, G. J. Nieuwenhuys, M. S. Rose, J. E. Sonier, B. Andraka, R. Chau, and M. B. Maple, Glassy Spin Dynamics in Non-Fermi-Liquid $UCu_{5-x}Pd_x$, $x = 1.0$ and 1.5, Phys. Rev. Lett. **87**, 066402 (2001).

[33] D. E. MacLaughlin, R. H. Heffner, O. O. Bernal, K. Ishida, J. E. Sonier, G. J. Nieuwenhuys, M. B. Maple, and G. R. Stewart, Disorder, inhomogeneity and spin dynamics in f-electron non-Fermi liquid systems, J. Phys.: Condens. Matter **16**, S4479 (2004).

[34] F. Gebhard, *The Mott Metal-Insulator Transition: Models and Methods*, Springer Series in Solid-State Sciences Vol. 137 (Springer, Berlin, 1997).

[35] P. Fazekas, *Lecture Notes on Electron Correlation and Magnetism*, Series in Modern Condensed Matter Physics (World Scientific, Singapore, 1999).

[36] M. Vekić, J. W. Cannon, D. J. Scalapino, R. T. Scalettar, and R. L. Sugar, Competition Between Antiferromagnetic Order and Spin-Liquid Behavior in the Two-Dimensional Periodic Anderson Model at Half Filling, Phys. Rev. Lett. **74**, 2367 (1995).

[37] W. Hu, R. T. Scalettar, E. W. Huang, and B. Moritz, Effects of an additional conduction band on the singlet-antiferromagnet competition in the periodic Anderson model, Phys. Rev. B **95**, 235122 (2017).

[38] T. Schäfer, A. A. Katanin, M. Kitatani, A. Toschi, and K. Held, Quantum criticality in the two-dimensional periodic Anderson model, arXiv:1812.03821.

[39] S. Doniach, The Kondo lattice and weak antiferromagnetism, Physica B&C **91**, 231 (1977).

[40] C. Lacroix and M. Cyrot, Phase diagram of the Kondo lattice, Phys. Rev. B **20**, 1969 (1979).

[41] P. Fazekas and E. Müller-Hartmann, Magnetic and nonmagnetic ground states of the Kondo lattice, Z. Phys. B **85**, 285 (1991).

[42] F. F. Assaad, Quantum Monte Carlo Simulations of the Half-Filled Two-Dimensional Kondo Lattice Model, Phys. Rev. Lett. **83**, 796 (1999).

[43] N. C. Costa, J. P. Lima, and R. R. dos Santos, Spiral magnetic phases on the Kondo lattice model: A Hartree-Fock approach, J. Magn. Magn. Mater. **423**, 74 (2017).

[44] M. Jiang, N. J. Curro, and R. T. Scalettar, Universal Knight shift anomaly in the periodic Anderson model, Phys. Rev. B **90**, 241109(R) (2014).

[45] M. Jiang and Y.-F. Yang, Universal scaling in the Knight-shift anomaly of the doped periodic Anderson model, Phys. Rev. B **95**, 235160 (2017).

[46] Similar results were also found in a closely related spin system, as reported in Ref. [63].

[47] A. Benali, Z. J. Bai, N. J. Curro, and R. T. Scalettar, Impurity-induced antiferromagnetic domains in the periodic Anderson model, Phys. Rev. B **94**, 085132 (2016).

[48] L.-Y. Wei and Y.-F. Yang, Doping-induced perturbation and percolation in the two-dimensional Anderson lattice, Sci. Rep. **7**, 46089 (2017).

[49] N. C. Costa, M. V. Araújo, J. P. Lima, T. Paiva, R. R. dos Santos, and R. T. Scalettar, Compressible ferrimagnetism in the depleted periodic Anderson model, Phys. Rev. B **97**, 085123 (2018).

[50] W. Wu and A. M.-S. Tremblay, d-Wave Superconductivity in the Frustrated Two-Dimensional Periodic Anderson Model, Phys. Rev. X **5**, 011019 (2015).

[51] L. Zhang, T. Ma, N. C. Costa, R. R. dos Santos, and R. T. Scalettar, Determinant quantum Monte Carlo study of exhaustion in the periodic Anderson model, arXiv:1903.09983.

[52] H. Sakai, F. Ronning, J.-X. Zhu, N. Wakeham, H. Yasuoka, Y. Tokunaga, S. Kambe, E. D. Bauer, and J. D. Thompson, Microscopic investigation of electronic inhomogeneity induced by substitutions in a quantum critical metal $CeCoIn_5$, Phys. Rev. B **92**, 121105(R) (2015).

[53] An early attempt to investigate the dPAM Hamiltonian was reported in Ref. [73].

[54] R. Blankenbecler, D. J. Scalapino, and R. L. Sugar, Monte Carlo calculations of coupled boson-fermion systems. I, Phys. Rev. D **24**, 2278 (1981).

[55] J. E. Hirsch, Two-dimensional Hubbard model: Numerical simulation study, Phys. Rev. B **31**, 4403 (1985).

[56] S. R. White, D. J. Scalapino, R. L. Sugar, E. Y. Loh, J. E. Gubernatis, and R. T. Scalettar, Numerical study of the two-dimensional Hubbard model, Phys. Rev. B **40**, 506 (1989).

[57] E. Y. Loh, J. E. Gubernatis, R. T. Scalettar, S. R. White, D. J. Scalapino, and R. L. Sugar, Sign problem in the numerical simulation of many-electron systems, Phys. Rev. B **41**, 9301 (1990).

[58] R. R. dos Santos, Introduction to quantum Monte Carlo simulations for fermionic systems, Braz. J. Phys. **33**, 36 (2003).

[59] M. Troyer and U.-J. Wiese, Computational Complexity and Fundamental Limitations to Fermionic Quantum Monte Carlo Simulations, Phys. Rev. Lett. **94**, 170201 (2005).

[60] N. J. Curro, B. Simovic, P. C. Hammel, P. G. Pagliuso, J. L. Sarrao, J. D. Thompson, and G. B. Martins, Anomalous NMR magnetic shifts in $CeCoIn_5$, Phys. Rev. B **64**, 180514(R) (2001).

[61] M. Raczkowski and F. F. Assaad, Emergent Coherent Lattice Behavior in Kondo Nanosystems, Phys. Rev. Lett. **122**, 097203 (2019).

[62] M. Charlebois, D. Sénéchal, A.-M. Gagnon, and A.-M. S. Tremblay, Impurity-induced magnetic moments on the graphene-lattice Hubbard model: An inhomogeneous cluster dynamical mean-field theory study, Phys. Rev. B **91**, 035132 (2015).

[63] T. Mendes-Santos, N. C. Costa, G. Batrouni, N. Curro, R. R. dos Santos, T. Paiva, and R. T. Scalettar, Impurities near an antiferromagnetic-singlet quantum critical point, Phys. Rev. B **95**, 054419 (2017).

[64] K. R. Shirer, A. C. Shockley, A. P. Dioguardi, J. Crocker, C. H. Lin, N. Roberts Warren, D. M. Nisson, P. Klavins, J. C. Cooley, Y.-F. Yang, and N. J. Curro, Long range order and two-fluid behavior in heavy electron materials, Proc. Natl. Acad. Sci. (USA) **109**, E3067 (2012).

[65] Y. Feng Yang, Two-fluid model for heavy electron physics, Rep. Prog. Phys. **79**, 074501 (2016).

[66] C. H. Lin, K. R. Shirer, J. Crocker, A. P. Dioguardi, M. M. Lawson, B. T. Bush, P. Klavins, and N. J. Curro, Evolution of hyperfine parameters across a quantum critical point in $CeRhIn_5$, Phys. Rev. B **92**, 155147 (2015).

[67] M. Randeria, N. Trivedi, A. Moreo, and R. T. Scalettar, Pairing and Spin Gap in the Normal State of Short Coherence Length Superconductors, Phys. Rev. Lett. **69**, 2001 (1992).

[68] R. K. Kaul and M. Vojta, Strongly inhomogeneous phases and non-Fermi-liquid behavior in randomly depleted Kondo lattices, Phys. Rev. B **75**, 132407 (2007).

[69] H. Watanabe and M. Ogata, Crossover from dilute-Kondo system to heavy-fermion system, Phys. Rev. B **81**, 113111 (2010).

[70] L. W. Cheuk, M. A. Nichols, M. Okan, T. Gersdorf, V. V. Ramasesh, W. S. Bakr, T. Lompe, and M. W. Zwierlein, Quantum-Gas Microscope for Fermionic Atoms, Phys. Rev. Lett. **114**, 193001 (2015).

[71] S. Kuhr, Quantum-gas microscopes: a new tool for cold-atom quantum simulators, Natl. Sci. Rev. **3**, 170 (2016).

[72] H. Ott, Single atom detection in ultracold quantum gases: a review of current progress, Rep. Prog. Phys. **79**, 054401 (2016).

[73] T. A. Costi, E. Müller-Hartmann, and K. A. Ulrich, Quantum Monte Carlo simulations of dilute and concentrated heavy-fermion systems, Solid State Commun. **66**, 343 (1988).